

On the electronic structure, bonding, spectra, and linear and nonlinear electric properties of Ti@C₂₈

Bartłomiej Skwara,[†] Robert W. Góra,^{*,†} Robert Zaleśny,[†] Paweł Lipkowski,[†]
Wojciech Bartkowiak,[†] Heribert Reis,[‡] Manthos G. Papadopoulos,^{*,‡} Josep M.
Luis,[¶] and Bernard Kirtman^{*,§}

Theoretical Chemistry Group, Institute of Physical and Theoretical Chemistry, Wrocław University of Technology, Wybrzeże Wyspiańskiego 27, 50-370 Wrocław, Poland, Institute of Organic and Pharmaceutical Chemistry, The National Hellenic Research Foundation, 48 Vas. Constantinou Avenue, 11635 Athens, Greece, Institute of Computational Chemistry, University of Girona, Campus de Montilivi, 17071 Girona, Catalonia, Spain and Department of Chemistry, University of Girona, Campus de Montilivi, 17071 Girona, Catalonia, Spain, and Department of Chemistry and Biochemistry, University of California, Santa Barbara, California 93106, USA

E-mail: robert.gora@pwr.wroc.pl; mpapad@eie.gr; kirtman@chem.ucsb.edu

*To whom correspondence should be addressed

[†]Theoretical Chemistry Group, Institute of Physical and Theoretical Chemistry, Wrocław University of Technology, Wybrzeże Wyspiańskiego 27, 50-370 Wrocław, Poland

[‡]Institute of Organic and Pharmaceutical Chemistry, The National Hellenic Research Foundation, 48 Vas. Constantinou Avenue, 11635 Athens, Greece

[¶]Institute of Computational Chemistry, University of Girona, Campus de Montilivi, 17071 Girona, Catalonia, Spain and Department of Chemistry, University of Girona, Campus de Montilivi, 17071 Girona, Catalonia, Spain

[§]Department of Chemistry and Biochemistry, University of California, Santa Barbara, California 93106, USA

Abstract

The potential energy surface of Ti@C₂₈ has been revisited and the stationary points have been carefully characterized. In particular, the C_{2v} symmetry structure considered previously turns out to be a transition state lying 2.3 kcal/mol above the ground state of C_{3v} symmetry at the MP2/6-31G(d) level. A large binding energy of 181.3 kcal/mol is found at the ROMP2/6-31G(d) level. Topological analysis of the generalized Ti@C₂₈ density reveals four bond paths between Ti and carbon atoms of the host. The character of all four contacts corresponds to a partially covalent closed shell interaction. UV-vis, IR and Raman spectra are calculated and compared with C₂₈H₄.

The dipole moment as well as the static electronic and double harmonic vibrational (hyper)polarizabilities have been obtained. Distortion of the fullerene cage due to encapsulation leads to non-zero diagonal components of the electronic first hyperpolarizability β , and to an increase in the diagonal components of the electronic polarizability α and second hyperpolarizability γ . However, introduction of the Ti atom causes a comparable or larger reduction in most cases due to localized bonding interactions.

At the double harmonic level, the average vibrational β is much larger than its electronic counterpart, but the opposite is true for α and for the contribution to γ that has been calculated. There is also a very large anharmonic (nuclear relaxation) contribution to β which results from a shallow PES with four minima separated by very low barriers. Thus, the vibrational γ (and α) may, likewise, become much larger when anharmonicity is taken into account.

July 1, 2011

INTRODUCTION

The ability of fullerenes to entrap atoms was revealed¹ soon after their discovery.² Until now, many endohedrally doped fullerenes have been synthesized³⁻⁵ and since they are a class of conjugated compounds their electric properties have been extensively studied theoretically and experimentally.⁶⁻¹⁷ Both atomic and small molecular species, such as transition metal atoms, noble gas atoms and methane, have been trapped inside carbon cages.^{6,18-28} It has been noted that charge transfer and covalent interactions between the fullerene and the encaged species may have a large effect on the electronic structure and properties of the resulting endohedral complex.^{6,29-34}

Among the various properties of interest, apart from structure and bonding, are the electronic and vibrational spectra as well as the linear and nonlinear (L&NLO) (hyper)polarizabilities.³⁵⁻⁴³ In addition to the pure electronic (hyper)polarizabilities an important consideration for the endohedral complexes is the contribution due to nuclear motion. Whitehouse and Buckingham predicted an exceptionally large vibrational contribution to the dipole polarizability of $[\text{C}_{60}\text{M}]^{n+}$ (where $\text{M}=\text{Li}, \text{Na}, \text{Mg}$) at temperatures above 20 K, assuming that the cage-ion potential surface is approximately flat.⁴⁴ This also implies that only a small field is required to move the ion from one side of the cage to the other. On the other hand, some of us have recently shown that within the nuclear relaxation approximation, and at 0 K, the vibrational contributions to the polarizability of $\text{Li}@\text{C}_{60}$ are rather modest.⁴⁵ It is of interest to see whether the same is true of $\text{Ti}@\text{C}_{28}$ and to examine the vibrational hyperpolarizabilities as well. To the best of our knowledge there have been no previous studies of the L&NLO properties of $\text{Ti}@\text{C}_{28}$. We also report for the first time, the theoretical UV-Vis, IR and Raman spectra of this system and compare these with the closed shell exohedral molecule C_{28}H_4 .

In order to elucidate the changes associated with encapsulation of the guest atom, it is helpful to compare selected properties not only with those of the above exohedral complex but also with the host molecule (C_{28}). Since all these systems have a relatively small size they can be studied using less approximate *ab initio* methods than in previous work. Although the electronic structure has been investigated, a number of aspects remain worthy of further exploration as will be evident from the following discussion.

C_{28} is one of the smallest fullerenes capable of encapsulating transition metal atoms.⁴⁶ *Ab initio* calculations have shown that it has an 5A_2 open shell ground state of T_d symmetry. This molecule can be considered as a superatom with an effective valency of four, both towards the outside and the inside of the cage. For C_{28} Guo *et al.*⁴⁷ found, at the HF level of theory and assuming C_{2v} symmetry, a set of low lying excited electronic states: 3A_2 , 3B_1 and 1A_1 . These were calculated to lie 1.6, 2.7 and 3.1 eV above the ground state. An isomer of C_{28} with D_2 symmetry was also obtained, but it is of considerably higher energy.⁴⁶

Although C_{28} appears to be even more abundant in the supersonic cluster beam produced by laser vaporization than C_{60} , it is very reactive. Thus, it can form particularly stable endohedral complexes with tetravalent metal atoms like Ti, Zr, Hf and U with relative abundances directly proportional to the size of the encapsulated atom.⁴⁶ It was suggested that this trend is associated with better spatial overlap of cage orbitals with the valence orbitals of larger atoms. Another way to chemically stabilize C_{28} is to saturate the four singly occupied, strongly electrophilic, p -like orbitals with four exohedral hydrogen atoms.^{48,49} This leads to the tetrahedral $C_{28}H_4$ molecule with a closed shell ground state.

In electronic structure calculations of $Ti@C_{28}$ T_d symmetry has usually been assumed.⁵⁰ However, Dunlap *et al.*^{51,52} have shown, through local density functional (LDA) calculations, that the Ti atom is not constrained to the center of the cage. In fact, the Ti atom is attracted significantly towards one of the four carbon atoms positioned in the corners of the tetrahedron (each with a singly occupied valence p -orbital in empty C_{28}). This would imply a lower symmetry structure with a threefold rotational symmetry. Later on Guo *et al.* considered a C_{2v} symmetry structure.⁴⁷ One of the objectives of this work is to perform more accurate *ab initio* calculations to characterize the C_{2v} and C_{3v} stationary points. Furthermore, an “Atoms in Molecules” (AIM) bonding analysis is carried out on the global minimum structure.

The remainder of this paper is organized in three sections. In the following section we present our computational methods. Then the results are discussed and, in the last section, the main conclusions are given.

COMPUTATIONAL METHODS

Electronic Properties

The structural and static electronic electric properties (dipole moment, polarizability, first- and second-order hyperpolarizability) of the studied systems were computed using second order Møller-Plesset perturbation theory with a restricted Hartree-Fock zeroth-order wavefunction, i.e. either closed shell (RMP2) or open shell (ROMP2) as appropriate. For the open shell case we used McWeeny and Diercksen canonicalization parameters.⁵³ For the selected properties of closed shell systems we used also the Kohn-Sham formulation of density functional theory (KS-DFT) with the BLYP, B3LYP and CAM-B3LYP exchange-correlation functionals. The choice of the ROHF reference wavefunction in calculations of C₂₈ was mainly due to high spin contamination in the Unrestricted Hartree-Fock (UHF) wavefunction and the large weight of the ROHF configuration in the CI wavefunction reported by Zhao and Pitzer.⁵⁴ It should be noted, however, that the arbitrariness in construction of the canonical Fock matrix leads to nonuniqueness in the perturbation theories based on the ROHF zeroth order wavefunction. Nevertheless, the resulting potential energy surfaces and other property surfaces are expected to be highly parallel. There is an excellent recent discussion of this subject by Glaesemann and Schmidt.⁵⁵ It should also be noted that for Ti@C₂₈ we observed UHF instabilities of the RHF wavefunction. Although such instabilities and high spin contamination usually indicate a fundamental shortcoming of the single determinant wavefunction description, previous studies suggest that, in the case of polycyclic aromatic hydrocarbons and linear polyenes, the R(O)MP2 method will yield energies and electric properties in relatively good agreement with highly electron-correlated methods,^{56–58} and the same may be expected for the systems studied here. Finally, for Ti@C₂₈ we performed single point CASSCF calculations to obtain several low lying singlet and triplet states using various active spaces and a small atomic natural orbital basis set. These calculations confirmed that the ground state is ¹A₁ and that it is well represented by the SCF wavefunction (the weight of the RHF configuration in all the CASSCF wavefunctions was always greater than 80% and the weights of the individual remaining

configurations were always smaller than 1%).

Since the ground state of Ti@C₂₈ is a closed shell singlet, and Ti is a 3d transition element, we believe that there is little need to account for relativistic effects in our calculations. Such an assumption is supported by recent studies of TiC in which the effect of scalar relativity on the computed spectroscopic constants including dipole moments was found to be quite small.⁵⁹ This greatly simplifies the computational treatment of Ti@C₂₈ in comparison with that of endohedral complexes with heavier tetravalent atoms.

Structural parameters were estimated using either the MP2 method with the 6-31G(d,p) basis set or KS-DFT with 6-31+G(d,p); all L&NLO property calculations (including electronic and vibrational spectra) were carried out with the 6-31+G(d,p) basis. MP2 calculations of electric properties using larger basis sets are cumbersome due to the size of the systems studied here. Therefore in order to investigate the effect of basis set extension we used the KS-DFT method with the B3LYP functional. The data reported in Table 1 indicate that the static electronic electric properties of Ti@C₂₈, computed here by means of the MP2 and B3LYP methods, with the 6-31+G(d) basis set, are consistent with each other and can be regarded as being of semi-quantitative accuracy.

The static electronic electric properties reported in this study were estimated by means of the finite field (FF) method with either the Rutishauser-Romberg (RR)⁶⁰ or Kurtz, *et al.*⁶¹ procedure. These properties are defined in terms of a Taylor series expansion of the energy in an external electric field (using the Einstein summation notation):

$$\begin{aligned}
 E(F) = E(0) - \mu_i F_i - \frac{1}{2!} \alpha_{ij} F_i F_j - \frac{1}{3!} \beta_{ijk} F_j F_k F_l - \\
 \frac{1}{4!} \gamma_{ijkl} F_i F_j F_k F_l + \dots
 \end{aligned}
 \tag{1}$$

$E(0)$ is the field independent energy, while μ_i , α_{ij} , β_{ijk} and γ_{ijkl} are the components of the dipole moment, polarizability, first hyperpolarizability and second hyperpolarizability tensors, respectively. All off-diagonal tensor elements were computed using the treatment of Ref. 61 with a base field of 0.001 a.u.

All diagonal property values were computed by employing the more accurate RR approach. For the latter a number of field strengths of magnitude $2^m F$ were used, where m denotes a set of consecutive integers and $F = 0.0001$ a.u. We have found that the region of stability falls in the range $F = 0.0008$ – 0.0016 a.u., which is why the base field 0.001 a.u. was used for the off-diagonal elements.

For the average properties we used:

$$\bar{\alpha} = \frac{1}{3} \sum_{i=x,y,z} \alpha_{ii} \quad (2)$$

$$\bar{\beta} = \sum_{i=x,y,z} \frac{\mu_i \beta_i}{|\mu|}, \quad (3)$$

where

$$\beta_i = \frac{1}{5} \sum_{j=x,y,z} (\beta_{ijj} + \beta_{jij} + \beta_{jji}), \quad (4)$$

and

$$\bar{\gamma} = \frac{1}{5} \sum_{ij=x,y,z} \gamma_{ijj}. \quad (5)$$

The calculated UV-Vis, IR and Raman spectra were plotted utilizing the open-source GAUSS-SUM routines.⁶²

Vibrational Contributions To Electric Dipole (Hyper)Polarizabilities

The total (hyper)polarizability for the non-rotating molecule can be divided into two contributions:⁶³

$$\mathbf{P} = \mathbf{P}^e + \mathbf{P}^{\text{vib}} \quad (6)$$

where \mathbf{P}^e and \mathbf{P}^{vib} denote the electronic (including the zero-point vibrational averaging (zpva) correction) and pure vibrational properties, respectively. For sake of simplicity we will drop the superscript “e” hereafter, unless it is necessary to distinguish electronic from vibrational contributions, and ignore the usually small zpva correction. \mathbf{P}^{vib} can be expressed as the sum of two

terms:⁶³

$$P^{\text{vib}} = P^{\text{nr}} + P^{\text{c-zpva}} \quad (7)$$

where P^{nr} is the nuclear relaxation contribution associated with the change in clamped nucleus electronic (without zpva) properties due to the change in equilibrium geometry induced by the field. $P^{\text{c-zpva}}$ (for notation see Ref. 64) is associated with the effect of the field-induced geometry relaxation on the corresponding zpva correction to the clamped nucleus electronic property values.⁶⁵ The latter term contains all remaining vibrational contributions not included in P^{nr} . It is usually smaller than the nuclear relaxation contribution^{66,67} and is not computed here. In the Bishop-Kirtman square bracket nomenclature the static ($\omega = 0$) P^{nr} properties are given by:⁶⁸

$$\alpha^{\text{nr}} = [\mu^2]_{\omega=0}^{0,0} \quad (8)$$

$$\beta^{\text{nr}} = [\mu\alpha]_{\omega=0}^{0,0} + [\mu^3]_{\omega=0}^{1,0} + [\mu^3]_{\omega=0}^{0,1} \quad (9)$$

$$\begin{aligned} \gamma^{\text{nr}} = & [\alpha^2]_{\omega=0}^{0,0} + [\mu\beta]_{\omega=0}^{0,0} + [\mu^2\alpha]_{\omega=0}^{0,1} + [\mu^2\alpha]_{\omega=0}^{1,0} + \\ & [\mu^4]_{\omega=0}^{2,0} + [\mu^4]_{\omega=0}^{0,2} + [\mu^4]_{\omega=0}^{1,1} \end{aligned} \quad (10)$$

The individual terms $[\]^{n,m}$, where n and m denote the order of electrical and mechanical anharmonicity, respectively, may be computed from energy, dipole moment and (hyper)polarizability derivatives.⁶⁸

The Bishop-Kirtman perturbation method, and the related nr treatment, is appropriate in the non-resonant regime wherein it is assumed that the laser optical frequencies may be neglected in comparison with electronic transition frequencies. Recently, a response formalism for computation of the terms that are thereby omitted has been presented.⁶⁹ However, it has now been shown that these missing terms vanish at both the static and infinite optical frequency limits, which are the cases studied here.⁷⁰

The vibrational contributions to the (hyper)polarizabilities were computed assuming the double harmonic approximation (in which only $[\]^{0,0}$ terms are retained in Eqs. (8-10)). In order to make a preliminary assessment of the anharmonicity contributions to hyperpolarizability, we also used

the finite-field approach proposed by Bishop, Hasan and Kirtman⁷¹ and developed by Luis et al.⁷²

All vibrational contributions to the (hyper)polarizabilities were estimated within the KS-DFT approach with the BLYP, B3LYP and CAM-B3LYP exchange-correlation potentials^{73–75} (as implemented in the GAUSSIAN 09⁷⁶ suite of programs) and the 6-31+G(d) basis set.

RESULTS AND DISCUSSION

Structural Properties

C_{28}

The equilibrium structure of the 5A_2 ground state of C_{28} was obtained at the ROMP2/6-31G(d) level of theory, assuming T_d symmetry and using analytical energy gradients as implemented in the GAMESS (US) package.⁷⁷ As pointed out by Guo *et al.*,⁴⁷ this structure has only three symmetry-distinct bond lengths (Figure 1). R_1 denotes the bond bridging the six-membered rings, R_2 is the bond within six-membered rings, and R_3 is the edge shared by two pentagons in the triplet of pentagons. In Table 2 we compare our results for the bond lengths with those obtained by Guo *et al.* at the HF/DZ level (probably UHF, though not specified).⁴⁷ Electron correlation influences the C_{28} structure significantly. In comparison with ROHF our ROMP2 R_1 and R_3 bonds are somewhat shorter, while the R_2 bond is elongated. For the sake of comparison we report also the corresponding UMP2 values, although these are less reliable due to high spin contamination.

$Ti@C_{28}$

The equilibrium structure of $Ti@C_{28}$ (see Figure 2), obtained at the RMP2/6-31G(d) level of theory, has C_{3v} symmetry. Guo *et al.*⁴⁷ reported a symmetry lowering to C_{2v} , but we found that the structure proposed and analyzed in their paper is, in fact, a first order saddle point that lies 2.3 kcal/mol above the global minimum. The C_{28} cage in the complex has nine distinguishable bond lengths with the Ti atom on the C_3 axis, 2.070 Å away from the C_1 carbon. Apart from the station-

ary points just mentioned, there are saddle points of C_{3v} and T_d symmetry, which are reported in the supplementary materials to this paper. These are located 7.1 and 47.8 kcal/mol, respectively, above the C_{3v} global minimum (MP2/6-31G(d) estimates).

In order to explain how the different stationary points are interconnected on the potential energy surface we would like to draw the reader's attention to the symmetry elements of an isolated C_{28} cage shown in Figure 1. This cage has the shape of a regular tetrahedron with four carbon atoms at the vertices and the central point (which we assume in this discussion to be the origin) has T_d symmetry. For the endohedral complex with Ti atom at the origin our calculations indicate that this point on the potential energy surface (PES) is a third order saddle point with triply degenerate imaginary frequencies of t_2 symmetry. The three normal modes correspond to displacements of Ti along the three C_2 symmetry axes passing through the origin and bisecting two opposite edges of the tetrahedron. This stationary point is a transition state that connects six equivalent C_{2v} symmetry stationary points and lies 45.5 kcal/mol above them. We have already pointed out that the C_{2v} stationary points, in turn, are first order transition states that connect two neighboring C_{3v} minima. There are four such minima, each of which may be generated by a displacement of the Ti atom from the origin along one of the four C_3 axes that pass through the vertex carbon atoms. In addition, there are four C_{3v} stationary positions where the Ti atom is displaced in the opposite direction along the C_3 axis. These are second order saddle points with imaginary frequencies of e symmetry (in the C_{3v} point group) and they connect three neighboring C_{3v} minima that lie in a plane parallel to a face of the tetrahedron. The saddle point is located 7.1 kcal/mol above the minima.

Although we report only the most accurate MP2/6-31G(d) results, the location of all the stationary points and their character was confirmed via fully analytical Hessian calculations using the HF and B3LYP methods. In the case of MP2 calculations we performed either analytical or semi-numerical (four point) Hessian calculations. Furthermore, we performed Intrinsic Reaction Coordinate (IRC) calculations at the HF/6-31G(d) level for all saddle points in order to determine the minimum energy paths and confirm our assignment.

Bonding Properties, Electronic and Vibrational Spectra of Ti@C₂₈

Binding Energy and Nature of Interactions

The binding energy (BE) of the endohedral complex in the 1A_1 ground state with respect to isolated 5A_2 C₂₈ and 3F_2 Ti ([Ar]d²s²) has been reported by Dunlap *et al.*⁵¹ at the LDA/VTZP level of theory and by Guo *et al.*⁴⁷ at the HF/DZ level of theory. In the former case, the value is 258.3 kcal/mol whereas in the latter it is -18.4 kcal/mol. This difference is remarkable, even taking into account that LDA tends to overestimate the BE contrary to the HF approximation, which usually underestimates this property. Our value for the binding energy of Ti@C₂₈ is 215.4 kcal/mol at the R(O)MP2/6-31G(d) level of approximation assuming McWeeny and Dierksen canonicalization parameters. When the Boys and Bernardi counterpoise correction⁷⁸ for the basis set superposition error at the equilibrium geometry is taken into account this value is reduced to 181.3 kcal/mol, which is our best estimate.

Such a large value of BE indicates strong chemical bonding between Ti and C₂₈. In order to gain more insight into the nature of this interaction we performed an AIM analysis (see Table 3), which is based on the topology of the electron density.⁷⁹⁻⁸² Our calculations were performed with the AIM 2000 program⁸³ using the generalized MP2 electron density to characterize the four bond paths formed between Ti and carbon atoms C₁-C₄ (indicated schematically in green on Figure 2). The Ti...C₁ interaction differs significantly from the remaining Ti...C₂₋₄ contacts, which are identical by symmetry. The distance to C₁ is shorter by about 0.02 Å and, as expected, the electron density at the bond critical point $\rho(r_{\text{BCP}})$ is greater (0.096 a.u. versus 0.089 a.u.). The larger value of the ellipticity, $\varepsilon(r_{\text{BCP}})$, for the C₂₋₄ bond paths implies greater distortion of the cylindrical shape of the electron density distribution, as in the case of double-bonds. In fact, the magnitude of the ellipticity in this case is larger than the corresponding $\varepsilon(r_{\text{BCP}})$ of ethylene.

An AIM analysis allows one to classify interactions as covalent, closed shell or somewhere in between, i.e. partially covalent, based on the Laplacian of the electron density $\nabla^2\rho(r_{\text{BCP}})$ and on the total energy density at the BCP ($H(r_{\text{BCP}})$). The latter is the sum of local kinetic ($G(r_{\text{BCP}})$)

and potential energy ($V(r_{\text{BCP}})$) densities. From the positive values of $\nabla^2\rho(r_{\text{BCP}})$ obtained for all Ti...C interactions we conclude that the interactions are of closed-shell character.⁸⁰ However, the values of $H(r_{\text{BCP}})$ are slightly negative indicating that the closed shell character is only partial and, therefore, that the four Ti...C interactions may be described as partially covalent in nature.⁸⁴ The molecular graph of Ti@C₂₈ is available in the supplement to this paper.

UV-Vis, IR and Raman Spectra of Ti@C₂₈ and Comparison with C₂₈H₄

Theoretical studies of the excited electronic states of C₂₈ and its endohedral complexes are scarce and usually limited to the analysis of orbital energy differences, particularly involving frontier orbitals.^{50–52,85} The most extensive analysis of the low lying electronic states of C₂₈ is that performed by Zhao and Pitzer.⁵⁴ These authors carried out limited singles and doubles spin-orbit CI calculations with improved virtual orbitals and found that, although the ⁵A₂ ground state is very well represented by the HF wavefunction, most of the excited states have large CI mixing. To our knowledge there are no existing theoretical investigations of excited electronic states of Ti@C₂₈ other than a single density of states calculation,⁸⁵ nor are there any experimental UV-Vis spectra of this system. The same is true of C₂₈H₄. In this work we fill that lacuna by calculating the UV-Vis spectrum of Ti@C₂₈ and its simplest exohedral counterpart (C₂₈H₄) within adiabatic time-dependent density functional theory (TDDFT).

A schematic spectrum for the first 200 states of Ti@C₂₈ was determined using the BLYP, B3LYP and CAM-B3LYP functionals and the 6-31G+(d) basis set at the MP2/6-31G(d) optimized geometry. The results shown in Figure 3, were obtained by convolution of the line positions with Gaussian functions assuming a full width at half-maximum of 3000 cm⁻¹. Our choice of the BLYP density functional was dictated by a previous report indicating a reasonable performance of nonhybrid functionals for prediction of electronic absorption spectra of fullerenes.⁸⁶ One should note, however, that TDDFT is applicable, in general, only to low-lying excited states that do not have appreciable double-excitation or charge-transfer character. In order to get some feeling for the effect of different functionals we decided to compare with hybrid B3LYP and the CAM-B3LYP

variant that has improved asymptotic behavior. All three functionals predict qualitatively similar spectra with the same origin of the most intense lines. However, the hybrid functionals predict that the main features will be slightly shifted towards shorter wavelength and also predict larger shifts of the less intense lines in the shoulder. Since there are no experimental data for comparison, in the following discussion we focus on the BLYP results and comment on the nature of the observed shifts.

The first excited state, which mainly involves the HOMO-LUMO transition, occurs at about 650 nm (1.909 eV). It is dipole forbidden like the majority of electronic transitions above 300 nm. The fact that the electronic spectrum is quenched in the long wavelength region is not surprising. This is, in fact, quite common in similar systems and is partially due to the high symmetry. For example in the C₆₀ fullerene there are sharp bands at about 213, 257 and 329 nm, but only weak features at higher wavelengths.⁸⁷

The most intense lines in Ti@C₂₈ appear at about 232 and 236 nm and are of *A*₁ and *E* symmetry respectively. For the sake of analysis recall that C₂₈ has tetrahedral symmetry with four carbon atoms at the vertices and a benzene-like hexagon of carbon atoms located at the four faces. It is convenient to adopt this tetrahedral structure as a basis for describing the molecular orbitals (MOs) of the encapsulated Ti system.⁵⁴ A linear combination of the vertex carbon *p* atomic orbitals (AOs) leads to *a*₁ and *t*₂ MOs. Under reduced C_{3v} symmetry, the latter splits into an *a*₁ plus an *e* pair. The main component of the 232 nm peak is due to a transition from the vertex *p*- π bonding MO of *a*₁ symmetry, with a significant contribution of Ti *d*_{z²}, to the π^* (*a*₁) MO composed of carbon *p*- π AOs on the hexagonal and pentagonal faces of C₂₈. On the other hand, the 236 nm ¹*E* transition is mainly due to excitation from the doubly degenerate vertex *p*- π + Ti *d* (*e*) orbitals to hexagon π^* MOs of *a*₁ and *a*₂ symmetry (see Figure 3a). These *A*₁ and *E* lines are shifted towards shorter wavelength by about 20 and 35 nm in the case of B3LYP and CAM-B3LYP, respectively. Thus, the observed shift is related to the proportion of exact exchange included in the hybrid functional (the amount of exact HF exchange in CAM-B3LYP increases throughout the long-range region). One observes also a corresponding shift of the 300 nm peak combined with a significant increase

of intensity. This is mainly due to several E and A_1 symmetry transitions similar in nature to the main feature (see supplementary materials for a more detailed version of the plot).

In order to further elucidate the effect of Ti encapsulation on the electronic spectrum of the endohedral complex we investigated, at the same level (BLYP and B3LYP), the simplest analogous closed shell exohedral system, namely tetrahedral $C_{28}H_4$. Our resultant schematic UV-Vis spectra are shown in Figure 3b. Interestingly, they are quite similar to those of the endohedral complex. Now, however, the two most intense lines in $Ti@C_{28}$ ($A_1 + E$) combine into a single line of T_2 symmetry with roughly the same oscillator strength as A_1 or E individually, and the line is shifted to shorter wavelength (217nm and 198 nm in the case of BLYP and B3LYP respectively). The main components of these transitions are due to excitations from the doubly degenerate $p-\pi$ (e) orbitals located on the C–C bonds joining two hexagons to π^* MOs of t_2 symmetry (see Figure 3b). On the other hand, there is also a T_2 transition at 328 nm, which is largely quenched in the spectrum of the endohedral complex, and another at 295 nm corresponding to the 282 nm peak of $Ti@C_{28}$ (BLYP results). Although the differences between the B3LYP and BLYP functionals are qualitatively the same as in the case of $Ti@C_{28}$, we note that the wavelength shifts as well as the observed increase of intensity are more pronounced for $C_{28}H_4$. Indeed, a comparison of the theoretical spectra of the endohedral and exohedral species indicates that the main effect associated with encapsulation of the Ti atom is the small red shift of the main feature and the associated increase of its intensity by roughly 20%. The latter arises mainly from an increased number of allowed, small intensity transitions due to the lowered symmetry. Unfortunately, there are no experimental data available for comparison.

Besides the electronic spectra we have also estimated the spectral frequencies, as well as IR and Raman intensities for the fundamental vibrations of $Ti@C_{28}$ and $C_{28}H_4$. These calculations were done using the B3LYP and CAM-B3LYP functionals with the 6-31+G(d) basis set. The resulting spectra, obtained by convolution of the line positions with Lorentzian curves assuming a full width at half-maximum of 10 cm^{-1} , are shown in Figure 4. Our numerical values as well as an assignment of the symmetry species of the corresponding vibrations can be found in the

supplementary material.

An extensive assessment of different DFT functionals for the prediction of vibrational frequencies, IR intensities and Raman activities of 122 molecules has been carried out by Jiménez-Hoyos et al.⁸⁸ They found that B3LYP and, to a slightly lesser extent, CAM-B3LYP performed very well for these quantities, if basis sets containing polarization and diffuse functions were employed, and the usual scaling factors were used for the harmonic frequencies. The good performance of B3LYP for IR intensities⁸⁹ and Raman activities⁹⁰ in comparison with high-level *ab-initio* results has also been reported by Halls and Schlegel. Thus, we may assume that the results reported here are reasonably accurate.

The B3LYP and CAM-B3LYP harmonic frequencies for Ti@C₂₈ are in good agreement. The root mean square deviation (RMS^a) between the unscaled frequencies is 27.8 cm⁻¹ (the corresponding average absolute deviation of CAM-B3LYP with respect to B3LYP is 1.5%) with a maximum absolute difference (MAD) of 44.6 cm⁻¹. For C₂₈H₄ the RMS deviation is quite similar, namely 27.2 cm⁻¹ (2.1%), with a MAD of 53.9 cm⁻¹. Generally, the discrepancies are larger at higher frequencies.

In the C_{3v} point-group of Ti@C₂₈ the modes of *a*₁ and *e* symmetry are both Raman and IR allowed. At the DFT level, the largest IR intensities are carried by the two high-frequency modes of *e* symmetry at 1357 and 1396 (1399 and 1437) cm⁻¹ at the B3LYP (CAM-B3LYP) levels. In addition, a cluster of 4 average intensity modes is found in the range 780–830 (765–852) cm⁻¹. The mode of lowest frequency, which occurs at 118 (108) cm⁻¹ and has *e* symmetry, may be described as a “rattling” of the Ti atom in the cage. It carries a fairly large IR intensity of 12.2 (14.6) km/mol, which is roughly the same as the intensity of the modes at 780–830 (765–852) cm⁻¹. For C₂₈H₄, only modes of *t*₂ symmetry are IR allowed leading to a comparatively simple spectrum with the two strongest peaks at 674 (677) and 787 (806) cm⁻¹.

By far the strongest Raman active vibration of Ti@C₂₈ is the cage breathing mode of *a*₁ symmetry that occurs at 726 (745) cm⁻¹ in the B3LYP (CAM-B3LYP) calculation. The corresponding

^aThe RMS was computed, as in Ref. 88 between symmetry-matched modes and degenerate modes were counted only once.

mode of $C_{28}H_4$ is shifted to 683 (699) cm^{-1} . Next most intense for $Ti@C_{28}$ (about 3.5 times weaker) is another a_1 mode at 979 (1008) cm^{-1} . The corresponding a_1 mode of $C_{28}H_4$ is shifted to higher frequencies, 1175 (1212) cm^{-1} with a significant increase of Raman activity (nearly 4 times). One should note, however, that the Raman spectrum of $C_{28}H_4$ is dominated by the nearly degenerate t_2 and a_1 hydrogen stretching frequencies at 3060 (\sim 3100) cm^{-1} .

As far as the vibrational contribution to the electric properties of $Ti@C_{28}$ is concerned, the most relevant difference between the endohedral and exohedral species (see later) is the low frequency degenerate e symmetry vibration of the former associated with large displacements of Ti within the cage.

Clamped Nucleus Electronic Contributions To Electrical Properties of $Ti@C_{28}$

The coordinate system employed for electrical property calculations of the $Ti@C_{28}$ complex in C_{3v} symmetry is shown in Figure 2 and (see later) Figure 5 (the Cartesian coordinates are provided in the supplementary materials). The z -axis is collinear with the principal C_3 symmetry axis and the Ti atom is at a distance of 0.4579 Å from an origin placed at the center of nuclear charge (or 0.4533 Å from the center of mass). This equilibrium geometry is in good agreement with the results of Dunlap *et al.*⁵¹

In Table 4 we present the diagonal components of the static electronic dipole moment and linear polarizability, as well as the first and second hyperpolarizability of C_{28} , $C_{28}H_4$ and $Ti@C_{28}$ at the equilibrium geometry. Except, perhaps, for the linear polarizability we see that electron correlation, estimated at the MP2 level, often has a significant effect on the computed property. For C_{28} two structures were investigated. The first is the true equilibrium T_d structure, while the second is the geometry this moiety assumes in the $Ti@C_{28}$ endohedral complex of C_{3v} symmetry. The reduction in symmetry for the latter leads to a non-zero average first hyperpolarizability. It also leads to an increase in the diagonal components of γ (ROMP2 level). (Note that $\beta_{xxx} = 0$ is not a consequence of symmetry but rather the (arbitrary) choice for the direction of the x -axis.)

Whereas encapsulation of Ti into the C_{3v} configuration of C_{28} leads to a small change in the

linear polarizability, there is a large reduction in the magnitude of the hyperpolarizabilities (MP2 level). This has been rationalized in other cases by invoking the orbital contraction (compression) effect.⁹¹⁻⁹⁴ On the other hand, we prefer an explanation based on the bonding interaction, and consequent localization, involving the four unpaired electrons within the C₂₈ cage. A comparison with C₂₈H₄ indicates that similar behavior is observed even though there can be no compression effect in that case.

Vibrational Contributions To Electrical Properties of Ti@C₂₈

In Table 5 we present several of the square bracket double harmonic vibrational contributions to the static (hyper)polarizabilities of Ti@C₂₈. The static electronic (hyper)polarizabilities are also included for comparison purposes. The values of the electronic properties obtained at the RHF level differ from those in Table 4 because different structures were used for the calculations. That is to say, the RMP2/6-31G(d) geometry was used for the data of Table 4, while the properties in Table 5 were calculated using geometries optimized at the same level of theory as the property calculations. This is necessary in order to correctly evaluate the vibrational (hyper)polarizabilities.

The data in Table 5 reveal some significant scatter between the various methods used to calculate the double harmonic vibrational terms. It is not straightforward to attribute the differences in DFT values to a specific feature of the exchange-correlation (XC) potential, particularly when the choice of basis set is so important as it is here. However, it is noticeable that for $\overline{[\mu^2]}$ and $\overline{[\mu\alpha]}$ the BLYP/6-31+G(d) and B3LYP/6-31+G(d) values are quite close to one another but differ substantially from the corresponding CAM-B3LYP value. Based on other systems⁹⁵ one might expect the CAM-B3LYP functional to be the preferred choice, but that is by no means definitive. Our results do suggest that, for these properties (and this system), the treatment of long-range exchange is important. On the other hand, the $\overline{[\alpha^2]}$ term is, surprisingly, almost independent of the XC functional.

For the first hyperpolarizability the double harmonic vibrational contribution to the average value (6-31+G(d) basis set) is much larger than the static electronic term. The largest contributions

to $\overline{[\mu\alpha]}_{\omega=0}^{0,0}$ are due to the xy , xxz and yyy components which, in turn, are dominated by the lowest-frequency degenerate pair of e symmetry vibrations shown in Figure 5. For instance, the B3LYP/6-31+G(d) value for the tensor element $[\mu\alpha]_{xxz}^{0,0}$ is 149 a.u. while the corresponding contribution from the e symmetry pair (at 120 cm^{-1}) is 147 a.u. On the other hand the largest contribution to $\overline{[\mu\alpha]}^{0,0}$ is due to the yyy component (the B3LYP/6-31+G(d) value is -341 a.u.) which is also largely determined by the two components of the e symmetry pair (the corresponding contribution to $[\mu\alpha]_{yyy}^{0,0}$ is -280 a.u.). The e vibration in question involves a particularly large displacement of the Ti atom with respect to the cage in the xy plane (in Figure 5 the two components have arbitrarily been oriented in the x and y directions). The potential energy surface for these modes is very shallow. To illustrate that point the B3LYP/6-31+G(d) energy profile for normal mode displacements of the e symmetry vibration is contrasted in Figure 6 with that of the $\nu_3(a_1)$ mode of frequency 394 cm^{-1} . The latter was chosen for this purpose because the normal mode displacements of the Ti atom (in this case along the C_3 axis) are also large.

In comparison with IR and Raman vibrational intensities the double harmonic expressions for vibrational (hyper)polarizabilities contain an additional weighting factor of $(\text{frequency})^{-2}$. That is why the vibrational modes corresponding to intense spectral features present in Figure 4 make relatively minor contributions to the double harmonic vibrational hyperpolarizabilities. It also explains why the 120 cm^{-1} e symmetry mode can make the dominant contribution to the first hyperpolarizability despite its very small Raman activity ($0.6\text{ \AA}^4/\text{amu}$) and why the 394 cm^{-1} a_1 symmetry vibration does not, even though the corresponding product of IR intensity (2.8 km/mol) and Raman activity ($9.6\text{ \AA}^4/\text{amu}$) is larger. It is reasonable to assume that the low frequency modes that dominate the double harmonic term will also make large anharmonicity contributions. Indeed, we have computed β_{yyy}^{nr} at the B3LYP/6-31+G(d) level of theory and it turns out to be 2.0×10^3 a.u., which is several times larger than the double harmonic value, and is associated with displacement of Ti along y axis that is an order of magnitude larger than for any of the carbon atoms.

Contrary to the case of the first hyperpolarizability, β , the double harmonic contribution to the components of the static α and γ ($[\alpha^2]$ term) are much smaller than the corresponding electronic

contribution. Nevertheless, the very large anharmonic contribution to β , which is a consequence of the flat PES landscape of Ti@C₂₈, suggests that the complete vibrational contribution to γ may be far larger than the double harmonic $[\alpha^2]$ term.

In addition to nuclear relaxation there is a pure vibrational contribution to the (hyper)polarizabilities that arises from higher order anharmonic effects, which is known as the c-zpva term. Again, because of the very flat PES, this term *may* be very large. However, its calculation presents some difficulties since the detailed shape of the PES with its four equivalent minima must be explicitly taken into account. Some of us have developed a new procedure for obtaining the c-zpva contribution in molecules with double minima⁹⁶ and we are currently working on the generalization to n equivalent minima. When that is done we plan to apply the new procedure to Ti@C₂₈.

It is of interest to compare the results found here with those obtained recently for Li@C₆₀. In both cases the double harmonic vibrational contribution to the static linear polarizability is small compared to the pure electronic term. On the other hand, for Li@C₆₀ the nuclear relaxation contributions to the static first and second hyperpolarizability are quite large.⁴⁵ This is consistent with what we have found for the static first hyperpolarizability of Ti@C₂₈. For the second hyperpolarizability only the $[\alpha^2]^{0,0}$ double harmonic term has been evaluated here. Although a more thorough comparison of the two endohedral fullerenes is desirable, it is beyond the scope of this paper and, indeed, is not feasible at the moment for several reasons: (i) a more extensive exploration of the Li@C₆₀ PES, as done here for Ti@C₂₈, is required; (ii) the level of theory applied thus far is different in the two cases; and (iii) a more complete treatment of anharmonicity, taking into account the c-zpva contribution, should be included.

CONCLUSIONS

We have determined the structure, dipole moment and (hyper)polarizabilities of C₂₈ and Ti@C₂₈ at various levels of approximation (HF, DFT, R(O)MP2). An “Atoms in Molecules” analysis of the interaction between the embedded Ti atom and the C₂₈ cage was carried out and the UV-Vis, IR

and Raman spectra were calculated for this endohedral fullerene. In addition, both electronic and (double harmonic) vibrational contributions to the static polarizability and hyperpolarizabilities were evaluated.

The major findings of the present work are as follows. Encapsulation of Ti in C_{28} lowers the symmetry from T_d to C_{3v} . There are transition states of C_{2v} and C_{3v} symmetry connecting the four equivalent minima that lie 2.3 and 7.1 kcal/mol, respectively, above the global minimum in MP2/6-31G(d) calculations. The position at the center of the cage is a third order transition state. It connects the six C_{2v} stationary points and lies 45.5 kcal/mol above them at the same MP2/6-31G(d) level of treatment. Our calculations confirm previous reports indicating that the endohedral complex is very stable: a binding energy of 181.3 kcal/mol is found for Ti@ C_{28} at the ROMP2/6-31G(d) level. Topological analysis of the generalized MP2 density reveals four bond paths between Ti and carbon atoms of the host corresponding to a partially covalent closed shell interaction.

The reduced symmetry of the fullerene cage due to encapsulation causes an increase in the diagonal components of the static electronic linear polarizability and second hyperpolarizability as well as non-zero values for the dipole moment and first hyperpolarizability. On the other hand, introduction of the Ti atom leads to localized bonding interactions and a consequent comparable or larger reduction in most cases for electrical properties other than the dipole moment.

Our preliminary B3LYP/6-31+G(d) calculations reveal that, in the double harmonic approximation, the static vibrational average first hyperpolarizability is much ($5\times$) larger than its electronic counterpart. When anharmonicity is considered the corresponding nuclear relaxation contribution to the major component is much larger than the double harmonic term ($6\times$). Otherwise, our calculations indicate that the double harmonic vibrational linear polarizability is relatively small compared to its pure electronic counterpart as is the $[\alpha^2]$ contribution to the second hyperpolarizability. Nevertheless, the flat potential energy surface, and the resulting very large anharmonic contribution to the first hyperpolarizability, indicate that the vibrational γ may exceed the corresponding electronic term when anharmonicity is taken into account. In addition to nuclear relax-

ation, the higher order c-zpva contribution may also be very substantial. Based on our treatment of double minimum potentials⁹⁶ we are currently developing methodology that will enable us to calculate this contribution for Ti@C₂₈, which has a PES with four equivalent minima that are separated by low energy barriers.

Since we believe that Ti@C₂₈ might be of interest for further experimental and theoretical studies we have carried out an extensive spectroscopic characterization including UV-Vis, IR, and Raman spectra estimated using the KS-DFT approach with a selection of functionals including BLYP, B3LYP and CAM-B3LYP. An analysis of the effect of encapsulation was done by comparing Ti@C₂₈ with C₂₈H₄.

Acknowledgement

The support from the European Union (MTKD-CT-2006-042488), and the computing resources from the Barcelona Supercomputing Center, TeraGrid (USA), DEISA (7th Framework Programme) and Wroclaw Center for Networking and Supercomputing are gratefully acknowledged. One of the authors (RZ) is the recipient of the fellowship co-financed by European Union within European Social Fund. RZ would also like to acknowledge support from a grant from Iceland, Liechtenstein and Norway through the EEA Financial Mechanism - Scholarship and Training Fund. MGP wishes to acknowledge funding received from the European Union's Seventh Framework Programme (FP7-REGPOT-2009-1) under grant agreement no. 245866, and the High-Performance Computing Infrastructure for South East Europe's Research Communities (HP-SEE), a project co-funded by the European Commission (under contract number 261499) through the Seventh Framework Programme.

Supporting Information Available

Supplementary data are available, including Cartesian coordinates of the stationary points, a more detailed plot of the calculated UV-vis spectrum, details of the calculated IR and Raman spectra, and the molecular graph of Ti@C₂₈. This material is available free of charge via the Internet at

<http://pubs.acs.org/>.

References

- (1) J. R. Heath and S. C. O'Brien and Q. Zhang and Y. Liu and R. F. Curl and H. W. Kroto and F. K. Tittel and R. E. Smalley, *J. Am. Chem. Soc.* **1985**, *107*, 7779–7780.
- (2) Kroto, H. W.; Heath, J. R.; O'Brien, S. C.; Curl, R. F.; Smalley, R. E. *Nature* **1985**, *318*, 162–163.
- (3) Chai, Y.; Guo, T.; Jin, C. M.; Haufler, R. E.; Chibante, L. P. F.; Fure, J.; Wang, L.; Alford, M.; Smalley, R. E. *J. Phys. Chem.* **1991**, *95*, 7564–7568.
- (4) Nagase, S.; Kobayashi, K.; Akasaka, T.; Wakahara, T. In *Fullerenes: Chemistry, Physics, and Technology*; Kadish, K. M., Ruoff, R. S., Eds.; John Wiley and Sons: New York, 2000; pp 395–436.
- (5) Akasaka, T., Nagase, S., Eds. *Endofullerenes: A New Family of Carbon Clusters*; Kluwer Academic Publishers: The Netherlands, 2002.
- (6) Shinohara, H. *Rep. Prog. Phys.* **2000**, *63*, 843–892.
- (7) Campbell, E.; Fanti, M.; Hertel, I.; Mitzner, R.; Zerbetto, F. *Chem. Phys. Lett.* **1998**, *288*, 131–137.
- (8) Gu, G.; Huang, H.; Yang, S.; Yu, P.; Fu, J.; Wong, G.; Wan, X.; Dong, J.; Du, Y. *Chem. Phys. Lett.* **1998**, *289*, 167–173.
- (9) Campbell, E. E. B.; Couris, S.; Fanti, M.; Koudoumas, E.; Krawez, N.; Zerbetto, F. *Adv. Mat.* **1999**, *11*, 405–408.
- (10) Antoine, R.; Rayane, D.; Benichou, E.; Dugourd, P.; Broyer, M. *Eur. Phys. J. D* **2000**, *12*, 147–151.
- (11) Torrens, F. *Nanotechnology* **2002**, *13*, 433–438.
- (12) Torrens, F. *J. Phys. Org. Chem.* **2002**, *15*, 742–749.

- (13) Xenogiannopoulou, E.; Couris, S.; Koudoumas, E.; Tagmatarchis, N.; Inoue, T.; Shinohara, H. *Chem. Phys. Lett.* **2004**, *394*, 14–18.
- (14) Tang, C.; Deng, K.; Tan, W.; Yuan, Y.; Liu, Y.; Wu, H.; Huang, D.; Hu, F.; Yang, J.; Wang, X. *Phys. Rev. A* **2007**, *76*, 013201.
- (15) Yan, H.; Yu, S.; Wang, X.; He, Y.; Huang, W.; Yang, M. *Chem. Phys. Lett.* **2008**, *456*, 223–226.
- (16) Yaghobi, M.; Rafie, R.; Koochi, A. *J. Mol. Struct. THEOCHEM* **2009**, *905*, 48–50.
- (17) He, J.; Wu, K.; Sa, R.; Li, Q.; Wei, Y. *Chem. Phys. Lett.* **2009**, *475*, 73–77.
- (18) Chai, Y.; Guo, T.; Jin, C.; Haufler, R. E.; Chibante, L. P. F.; Fure, J.; Wang, L.; Alford, J. M.; Smalley, R. E. *J. Phys. Chem.* **1991**, *95*, 7564.
- (19) Manolopoulos, D. E.; Fowler, P. W. *Chem. Phys. Lett.* **1991**, *187*, 12.
- (20) Bethune, D. S.; Johnson, R. D.; Salem, J. R.; de Vries, M. S.; Yannoni, C. S. *Nature* **1993**, *366*, 123.
- (21) Beyers, R.; Kiang, C. H.; Johnson, R. D.; Salem, J. R.; de Vries, M. S.; Yannoni, C. S.; Bethune, D. S.; Dorn, H. C.; Burbank, P.; Harich, K.; Stevenson, S. *Nature* **1994**, *370*, 196.
- (22) Fowler, P.; Manolopoulos, D. E. *An Atlas of Fullerenes*; Oxford Univ. Press, 1995.
- (23) Kobayashi, K.; Nagase, S. *Chem. Phys. Lett.* **1996**, *262*, 227.
- (24) Saunders, M.; Cross, R. J.; Jimenez Vazquez, H. A.; Shimshi, R.; Khong, A. *Science* **1996**, *271*, 1693–1697.
- (25) Guha, S.; Nakamoto, K. *Coord. Chem. Rev.* **2005**, *249*, 1111.
- (26) Dunsch, L.; Yang, S. *Electrochem. Soc. Interface* **2006**, *15*, 34.
- (27) Rehaman, A.; Gagliardi, L.; Pyykkö, P. *Int. J. Quantum Chem.* **2007**, *107*, 1162.

- (28) Infante, I.; Gagliardi, L.; Scuseria, G. E. *J. Am. Chem. Soc.* **2008**, *130*, 7459.
- (29) Cioslowski, J.; Fleischmann, E. D. *J. Chem. Phys.* **1991**, *94*, 3730–3734.
- (30) Cioslowski, J. *J. Am. Chem. Soc.* **1991**, *113*, 4139–4141.
- (31) Ross, M. M.; Nelson, H. H.; Callahan, J. H.; McElvany, S. W. *J. Phys. Chem.* **1992**, *96*, 5231.
- (32) Campanera, J. M.; Bo, C.; Olmstead, M. M.; Balch, A. L.; Poblet, J. M. *J. Phys. Chem. A* **2002**, *106*, 12356.
- (33) Nádai, C. D.; Mirone, A.; Dhesi, S. S.; Bencok, P.; Brookes, N. B.; Marenne, I.; Rudolf, P.; Tagmatarchis, N.; Shinohara, H.; Dennis, T. J. S. *Phys. Rev. B* **2004**, *69*, 184421.
- (34) Park, S. S.; Liu, D.; Hagelberg, F. *J. Phys. Chem. A* **2005**, *109*, 8865.
- (35) Luo, Y.; Norman, P.; Macak, P.; Ågren, H. *Phys. Rev. B* **2000**, *61*, 3060.
- (36) Jensen, L.; Åstrand, P. O.; Mikkelsen, K. V. *J. Phys. Chem. B* **2004**, *108*, 8226.
- (37) Xie, R. H.; Rao, Q.; Jensen, L. In *Encyclopedia of Nanoscience and Nanotechnology*; Nalwa, H. S., Ed.; American Scientific: Stevenson Ranch, CA, 2004; p 67.
- (38) Jensen, L.; Åstrand, P. O.; Osted, A.; Kongsted, J.; Mikkelsen, K. V. *J. Chem. Phys.* **2002**, *116*, 4001.
- (39) van Gisbergen, S. J. A.; Snijders, J. G.; Baerends, E. J. *Phys. Rev. Lett.* **1997**, *78*, 3097.
- (40) Jonsson, D.; Norman, P.; Ruud, K.; Ågren, H. *J. Chem. Phys.* **1998**, *109*, 572.
- (41) Talapatra, G. B.; Manickam, N.; Samoć, M.; Orczyk, M.; Karna, S. P.; Prasad, P. N. *J. Phys. Chem.* **1992**, *96*, 5206.
- (42) Thole, B. T. *Chem. Phys.* **1981**, *59*, 341.
- (43) Jensen, L.; van Duijnen, P. T. *Int. J. Quantum Chem.* **2005**, *102*, 612.

- (44) Whitehouse, D. B.; Buckingham, A. D. *Chem. Phys. Lett.* **1993**, *207*, 332.
- (45) Reis, H.; Loboda, O.; Avramopoulos, A.; Papadopoulos, M. G.; Kirtman, B.; Luis, J. M.; Zaleśny, R. *J. Comp. Chem.* **2010**, *32*, 908–914.
- (46) Guo, T.; Diener, M.; Cai, Y.; Alford, M. J.; Haufler, R. E.; McClure, S. M.; Ohno, T.; Weaver, J. H.; Scuseria, G. E.; Smalley, R. E. *Science* **1992**, *257*, 1661.
- (47) Guo, T.; Smalley, R. E.; Scuseria, G. E. *J. Chem. Phys.* **1993**, *99*, 352.
- (48) Fayereisen, M.; Gutowski, M.; Simons, J.; Almlöf, J. *J. Chem. Phys.* **1992**, *96*, 2926.
- (49) Zhao, X.; Lu, P.; Hao, C.; Li, S.; Qiu, J. *J. Mol. Struct. THEOCHEM* **2006**, *760*, 53 – 57.
- (50) Makurin, Y. N.; Sofronov, A. A.; Gusev, A. I.; Ivanovsky, A. L. *Chem. Phys.* **2001**, *270*, 293.
- (51) Dunlap, B. I.; Häberlen, O. D.; Rösch, N. *J. Phys. Chem.* **1992**, *96*, 9095.
- (52) Häberlen, O. D.; Rösch, N.; Dunlap, B. I. *Chem. Phys. Lett.* **1992**, *200*, 418.
- (53) McWeeny, R.; Diercksen, G. *J. Chem. Phys.* **1968**, *49*, 4852–4856.
- (54) Zhao, K.; Pitzer, R. M. *J. Phys Chem.* **1996**, *100*, 4798.
- (55) Glaesemann, K. R.; Schmidt, M. W. *J. Phys. Chem. A* **2010**, *114*, 8772–8777.
- (56) Colvin, M.; Janssen, C.; Seidl, E.; Nielsen, I.; Melius, C. *Chem. Phys. Lett.* **1998**, *287*, 537–541.
- (57) Smith, S.; Markevitch, A.; Romanov, D.; Li, X.; Levis, R.; Schlegel, H. *J. Phys. Chem. A* **2004**, *108*, 11063–11072.
- (58) Champagne, B.; Botek, E.; Nakano, M.; Nitta, T.; Yamaguchi, K. *J. Chem. Phys.* **2005**, *122*, 114315.
- (59) Jr, C. W. *Theo. Chem. Acc.* **2003**, *110*, 153–155.

- (60) Rutishauser, H. *Numerische Mathematik* **1963**, *5*, 48–54.
- (61) Kurtz, H. A.; Stewart, J. J. P.; Dieter, K. M. *J. Comput. Chem.* **1990**, *11*, 82.
- (62) O’Boyle, N. M.; Tenderholt, A. L.; Langner, K. M. *J. Comput. Chem.* **2008**, *29*, 839–845.
- (63) Bishop, D. *Adv. Chem. Phys.* **1998**, *104*, 1–40.
- (64) Kirtman, B.; Luis, J. In *Non-Linear Optical Properties of Matter, From Molecules to Condensed Phases*; Papadopoulos, M., Sadlej, A., Leszczynski, J., Eds.; Springer, 2006; p 101128.
- (65) Kirtman, B.; Luis, J. M.; Bishop, D. M. *J. Chem. Phys.* **1998**, *108*, 10008.
- (66) Torrent-Sucarrat, M.; Sola, M.; Duran, M.; Luis, J. M.; Kirtman, B. *J. Chem. Phys.* **2002**, *116*, 5363.
- (67) Jug, K.; Chiodo, S.; Calaminici, P.; Avramopoulos, A.; Papadopoulos, M. G. *J. Phys. Chem. A* **2003**, *107*, 4172.
- (68) Kirtman, B.; Champagne, B.; Luis, J. M. *J. Comp. Chem.* **2000**, *16*, 1572.
- (69) M. B. Hansen and O. Christiansen and C. Hättig, *J. Chem. Phys.* **2009**, *131*, 154101.
- (70) B. Kirtman and J. M. Luis, *Int. J. Quant. Chem.* **2011**, *111*, 839.
- (71) Bishop, D. M.; Hasan, M.; Kirtman, B. *J. Chem. Phys.* **1995**, *103*, 4157–4159.
- (72) Luis, J. M.; Duran, M.; Andrés, J. L.; Champagne, B.; Kirtman, B. *J. Chem. Phys.* **1999**, *111*, 875–884.
- (73) Becke, A. D. *Phys. Rev. A* **1988**, *38*, 3098–3100.
- (74) Lee, C.; Yang, W.; Parr, R. G. *Phys. Rev. B* **1988**, *37*, 785–789.
- (75) Yanai, T.; Tew, D. P.; Handy, N. C. *Chem. Phys. Lett.* **2004**, *393*, 51–57.

- (76) Frisch, M. J. et al. GAUSSIAN 09 Revision A.1. Gaussian Inc. Wallingford CT 2009.
- (77) Schmidt, M. W.; Baldridge, K. K.; Boatz, J. A.; Elbert, S. T.; Gordon, M. S.; Jensen, J. H.; Koseki, S.; Matsunaga, N.; Nguyen, K. A.; Su, S.; Windus, T. L.; Dupuis, M.; Montgomery, J. A. *J. Comput. Chem.* **1993**, *14*, 1347–1363.
- (78) Boys, S. F.; Bernardi, F. *Mol. Phys.* **1970**, *19*, 553–566.
- (79) Bader, R. F. W. *Atoms In Molecules, A Quantum Theory*; Oxford University Press: Oxford, 1990.
- (80) Bader, R. F. W. *Chem. Rev.* **1991**, *91*, 893.
- (81) Popelier, P. *Atoms in Molecules, An Introduction*; Pearson Education Ltd: Prentice Hall, 2000.
- (82) Matta, C. F.; (eds), R. J. B. *The Quantum Theory of Atoms in Molecules: Sfrom Solid State to DNA and Drug Design*; Wiley VCH: Weinheim, 2007.
- (83) designed by Friedrich Biegler-Konig, AIM2000 package. University of Applied Sciences, Bielefeld, Germany.
- (84) Espinosa, E.; Alkorta, I.; Elguero, J.; Molins, E. *J.Chem.Phys.* **2002**, *117*, 5529.
- (85) Jackson, K.; Kaxiras, E.; Pederson, M. R. *Phys. Rev. B* **1993**, *48*, 17556.
- (86) Bauernschmitt, R.; Ahlrichs, R.; Hennrich, F.; Kappes, M. *J. Am. Chem. Soc.* **1998**, *120*, 5052–5059.
- (87) Hare, J. P.; Kroto, H. W.; Taylor, R. *Chem. Phys. Lett.* **1991**, *177*, 394.
- (88) Jiménez-Hoyos, C. A.; Janesko, B. G.; Scuseria, G. E. *Phys. Chem. Chem. Phys.* **2008**, *10*, 6621.
- (89) Hall, M. D.; Schlegel, H. B. *J. Chem. Phys.* **1998**, *109*, 10587.

- (90) Hall, M. D.; Schlegel, H. B. *J. Chem. Phys.* **1999**, *111*, 8819.
- (91) Papadopoulos, M. G.; Sadlej, A. J. *Chem. Phys. Lett.* **1998**, *288*, 377.
- (92) Fowler, P. W.; Madden, P. A. *Phys. Rev. B* **1984**, *29*, 1035.
- (93) Fowler, P. W. *J. Phys. Chem.* **1985**, *89*, 2581.
- (94) Kaczmarek, A.; Bartkowiak, W. *Phys. Chem. Chem. Phys.* **2009**, *11*, 2885.
- (95) Zaleśny, R.; Bulik, I. W.; Bartkowiak, W.; Luis, J. M.; Avramopoulos, A.; Papdopoulos, M. G.; Krawczyk, P. *J. Chem. Phys.* **2010**, *133*, 244308.
- (96) Luis, J. M.; Reis, H.; Papadopoulos, M.; Kirtman, B. *J. Chem. Phys.* **2009**, *131*, 034116.

Tables

Table 1: Selected components of the static electronic electric dipole moment and (hyper)polarizabilities (in a.u.) of Ti@C₂₈ estimated using the B3LYP and MP2 methods with various basis sets. Electric properties were estimated from fits of finite field calculations using the Rutishauser-Romberg approach. The MP2/6-31G(d) equilibrium geometry was assumed in all calculations.

	μ_z	α_{zz}	β_{zzz}	γ_{zzzz}
MP2/6-31G(d)	0.921	220.34	-262.9	12.5×10^3
MP2/6-31+G(d)	1.088	258.83	23.1	103.7×10^3
B3LYP/6-31+G(d)	1.214	250.88	38.4	83.3×10^3
B3LYP/aug-cc-pVDZ	1.207	252.73	52.8	78.2×10^3
B3LYP/aug-cc-pVTZ	1.179	252.56	55.3	78.0×10^3

Table 2: Structural parameters of C_{28} (T_d). Bond lengths, defined in Figure 1, are in Ångstroms.

	R_1	R_2	R_3
HF/DZ ^a	1.538	1.397	1.482
ROHF/6-31G(d)	1.511	1.403	1.475
UMP2/6-31G(d)	1.419	1.407	1.443
ROMP2/6-31G(d)	1.499	1.440	1.434

a) Guo *et al.*⁴⁷

Table 3: AIM topological properties (given in a.u.) of the Ti...C bond critical points in the Ti@C₂₈ endohedral complex.

BCP	$R_{\text{Ti}\dots\text{C}}$	$\rho(r_{\text{BCP}})$	$\nabla^2\rho(r_{\text{BCP}})$	$V(r_{\text{BCP}})$	$G(r_{\text{BCP}})$	$H(r_{\text{BCP}})$	$\varepsilon(r_{\text{BCP}})$
Ti...C ₁	2.069	0.096	0.283	-0.126	0.098	-0.028	0.000
Ti...C ₂₋₄	2.087	0.089	0.294	-0.120	0.097	-0.023	0.719

Table 4: Static diagonal components of the electronic electric dipole moment and (hyper)polarizabilities^{b)} (in a.u.) of Ti@C₂₈, C₂₈H₄ and two structures of C₂₈. These values were estimated using the Rutishauser-Romberg procedure and 6-31+G(d,p) basis set.

	Ti@C ₂₈ (C _{3v})		C ₂₈ (C _{3v}) ^{a)}		C ₂₈ (T _d)		C ₂₈ H ₄ (T _d)	
	RHF	RMP2	ROHF	ROMP2	ROHF	ROMP2	RHF	RMP2
μ_x	0.000	0.000	0.000	0.000	0.000	0.000	0.000	0.000
μ_z	1.612	1.088	-0.009	-0.055	0.000	0.000	0.000	0.000
α_{xx}	267.20	275.96	254.92	277.40	251.33	265.30	246.59	251.06
α_{zz}	245.81	258.83	258.94	281.04	251.33	265.30	246.59	251.06
β_{xxx}	0.0	0.0	0.0	0.0	0.0	0.0	0.0	0.0
β_{yyy}	-33.9	-126.6	-40.6	-192.0	0.0	0.0	0.0	0.0
β_{zzz}	117.3	23.1	-92.0	-588.4	0.0	0.0	0.0	0.0
$\gamma_{xxx} \times 10^{-3}$	96.2	119.5	101.8	149.6	96.6	127.0	72.0	104.0
$\gamma_{zzz} \times 10^{-3}$	79.3	103.7	99.9	141.2	96.6	127.0	72.0	104.0

a) Carbon cage geometry corresponding to rigid removal of Ti from Ti@C₂₈

b) For the systems studied, and axes as defined, $\mu_y = \mu_x$, $\alpha_{yy} = \alpha_{xx}$ and $\gamma_{yyy} = \gamma_{xxx}$.

Table 5: Static electronic and double harmonic vibrational terms that contribute to the (hyper)polarizability^{b)} of Ti@C₂₈ (in a.u.), as calculated by the RHF and several DFT methods using the 6-31+G(d) and 6-31G(d) (values in square brackets) basis sets.^{a)}

	BLYP	B3LYP	CAM-B3LYP	RHF
α_{xx}^e	272.0	264.4	258.7	258.4
α_{zz}^e	259.9	250.0	241.8	238.6
$\bar{\alpha}^e$	267.9 [229.1]	259.6 [223.6]	253.1 [218.3]	251.8 [216.6]
$[\mu^2]_{xx,\omega=0}^{0,0}$	21.2	27.1	38.0	58.1
$[\mu^2]_{zz,\omega=0}^{0,0}$	4.2	3.9	3.8	4.7
$[\overline{\mu^2}]_{\omega=0}^{0,0}$	15.5 [9.7]	19.3 [13.9]	26.5 [20.4]	40.3 [34.9]
β_{xxx}^e	0.0	0.0	0.0	0.0
β_{yyy}^e	-71.2	-65.7	-66.6	-66.5
β_{zzz}^e	4.3	25.5	61.3	98.6
$\bar{\beta}^e$	7.6 [-360.6]	-10.4 [-347.2]	-14.1 [-333.5]	-34.4 [-345.1]
$[\mu\alpha]_{xxx,\omega=0}^{0,0}$	0.0	0.0	0.0	0.0
$[\mu\alpha]_{yyy,\omega=0}^{0,0}$	-273.5	-341.4	-448.5	-673.0
$[\mu\alpha]_{zzz,\omega=0}^{0,0}$	6.5	27.4	43.1	69.4
$[\overline{\mu\alpha}]_{\omega=0}^{0,0}$	196.2 [223.9]	195.3 [277.0]	275.9 [417.6]	175.4 [438.6]
γ_{xxxx}^e	110×10^3	98×10^3	85×10^3	94×10^3
γ_{zzzz}^e	92×10^3	81×10^3	70×10^3	74×10^3
$\bar{\gamma}^e$	103×10^3 [6×10^3]	91×10^3 [6×10^3]	79×10^3 [5×10^3]	87×10^3 [7×10^3]
$[\alpha^2]_{xxxx,\omega=0}^{0,0}$	24×10^3	23×10^3	22×10^3	23×10^3
$[\alpha^2]_{zzzz,\omega=0}^{0,0}$	18×10^3	16×10^3	14×10^3	14×10^3
$[\overline{\alpha^2}]_{\omega=0}^{0,0}$	21×10^3 [17×10^3]	19×10^3 [15×10^3]	19×10^3 [15×10^3]	19×10^3 [15×10^3]

^{a)} All calculations in this table were performed at the geometry obtained for the corresponding quantum chemical method.

^{b)} For the systems studied, and the definition of axes, $\alpha_{yy}^e = \alpha_{xx}^e$, $[\mu^2]_{yy,\omega=0}^{0,0} = [\mu^2]_{xx,\omega=0}^{0,0}$, $\gamma_{yyyy}^e = \gamma_{xxxx}^e$ and $[\alpha^2]_{yyyy,\omega=0}^{0,0} = [\alpha^2]_{xxxx,\omega=0}^{0,0}$.

Figures

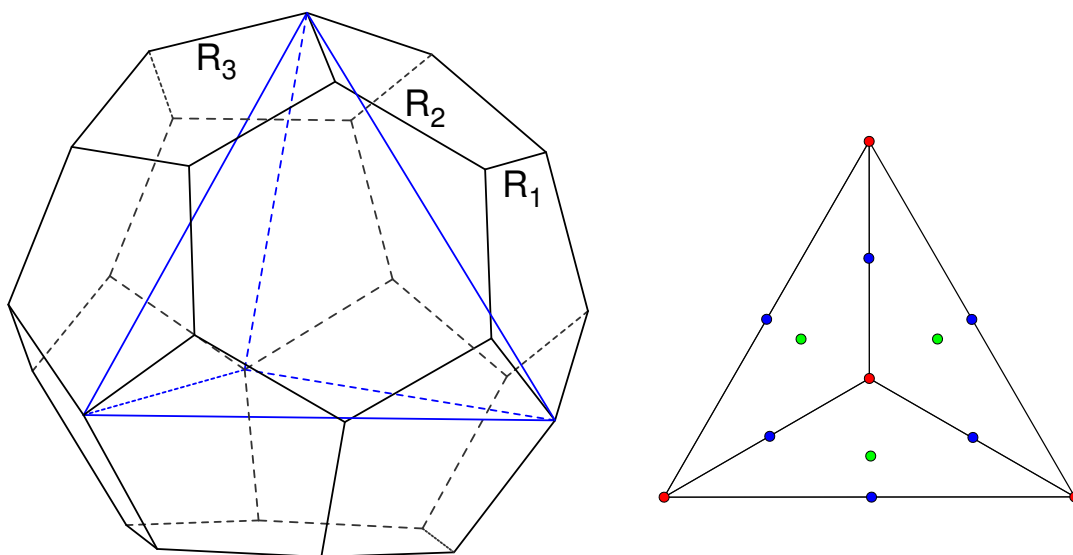


Figure 1: The structure of C_{28} with inscribed tetrahedron indicating its T_d point group symmetry (left). On the right we plot the projection of tetrahedron showing schematically the relevant positions of the guest atom and the corresponding point group symmetries of endohedral complex. In the case of $Ti@C_{28}$ the red dots correspond to C_{3v} minima, the green dots on the faces of tetrahedron indicate the C_{3v} transition states and the blue dots represent the C_{2v} transition states.

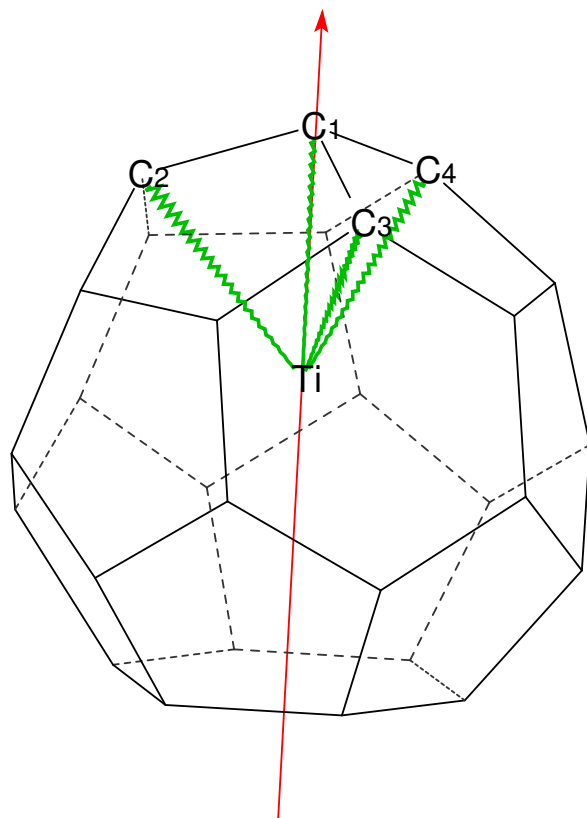


Figure 2: The structure of Ti@C₂₈. The principal symmetry axis C₃ (z) is shown in red and the schematic QTAIM bond paths are indicated in green. See text for the discussion.

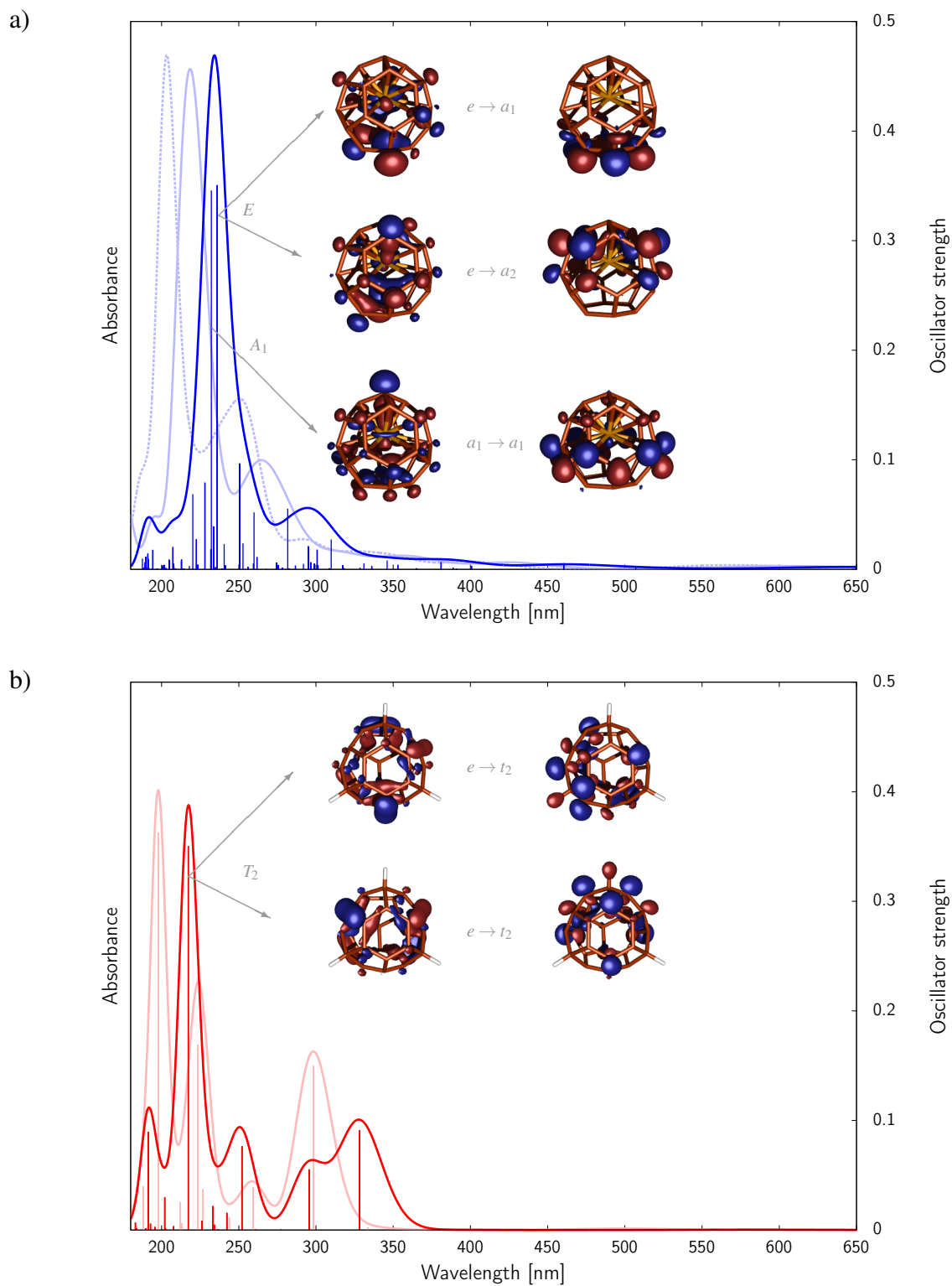


Figure 3: The UV-Vis spectra of Ti@C_{28} (a) and C_{28}H_4 (b) computed by means of the adiabatic TDDFT method using BLYP (solid dark), B3LYP (solid light) and CAM-B3LYP (dashed) exchange-correlation functionals and 6-31G+(d,p) basis set at the optimized MP2/6-31G(d,p) geometry.

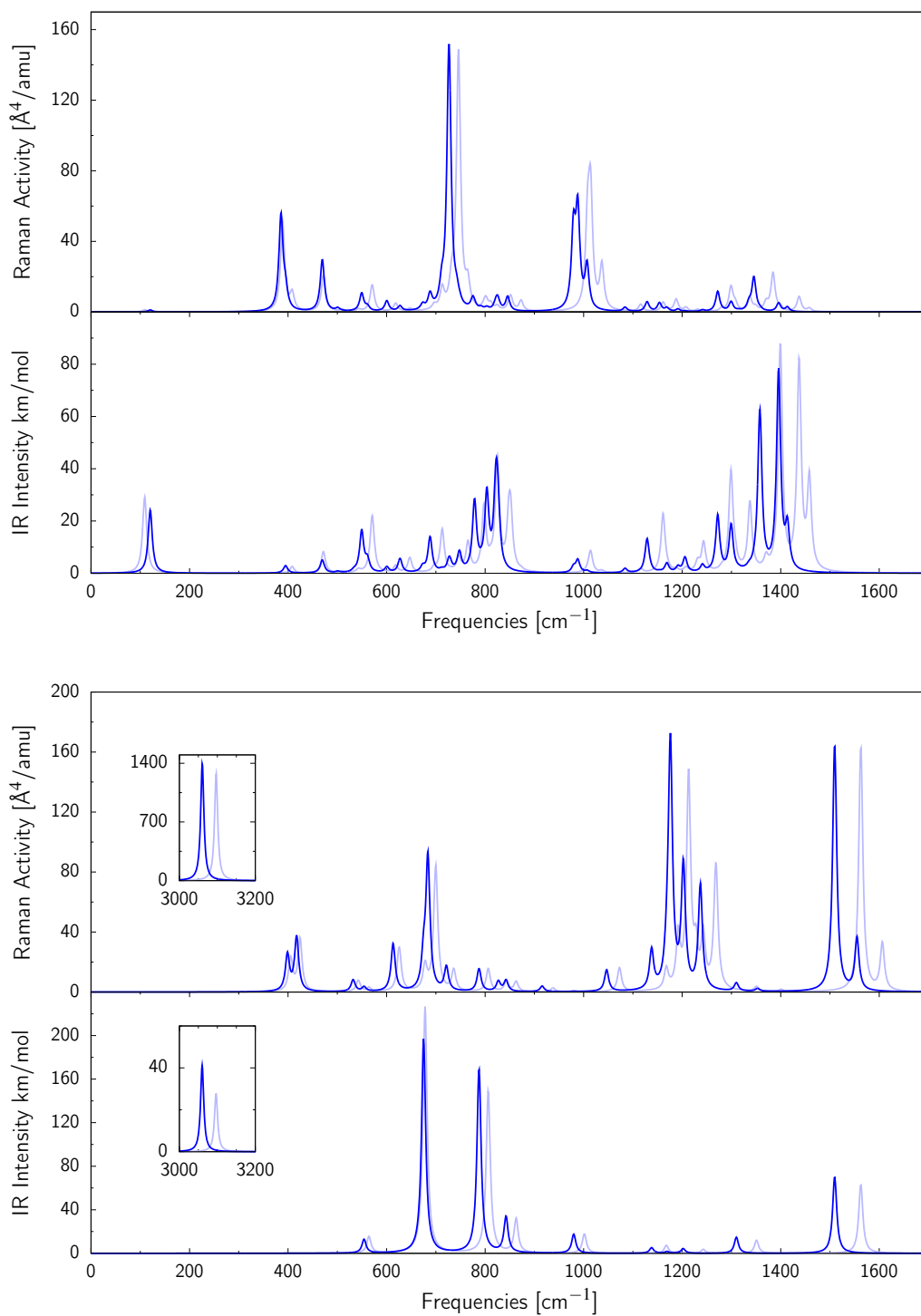


Figure 4: The IR and Raman spectra of Ti@C₂₈ (top) and C₂₈H₄ (bottom) computed within harmonic approximation using B3LYP (dark blue) and CAM-B3LYP (light blue) methods and 6-31G+(d,p) basis set. The insets show the C-H stretching bands above 3000 cm⁻¹ that are present only in C₂₈H₄.

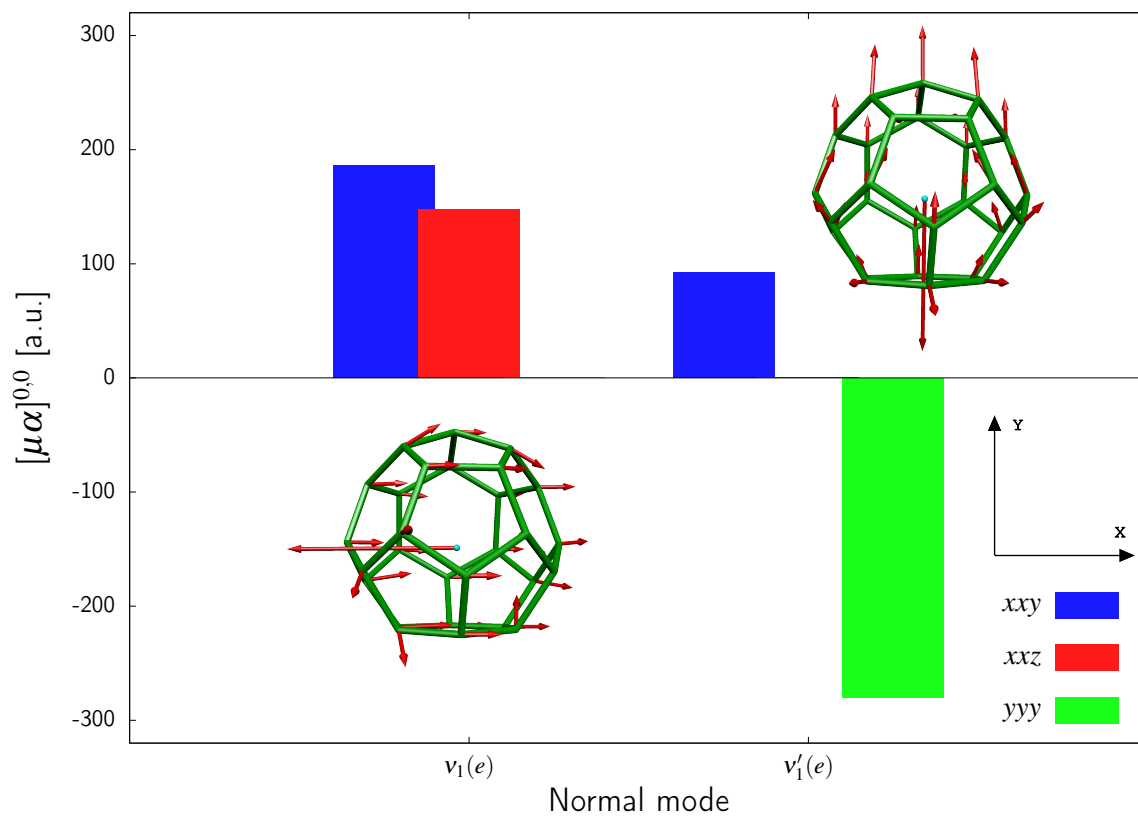


Figure 5: The two components of the low-frequency e symmetry normal mode of Ti@C_{28} discussed in text and their contributions to the tensor elements of $[\overline{\mu\alpha}]^{0,0}$. Please note that the orientation of the molecular frame is different than in Figure 2 and the principal C_3 (z) axis now goes through the carbon atom closest to the reader.

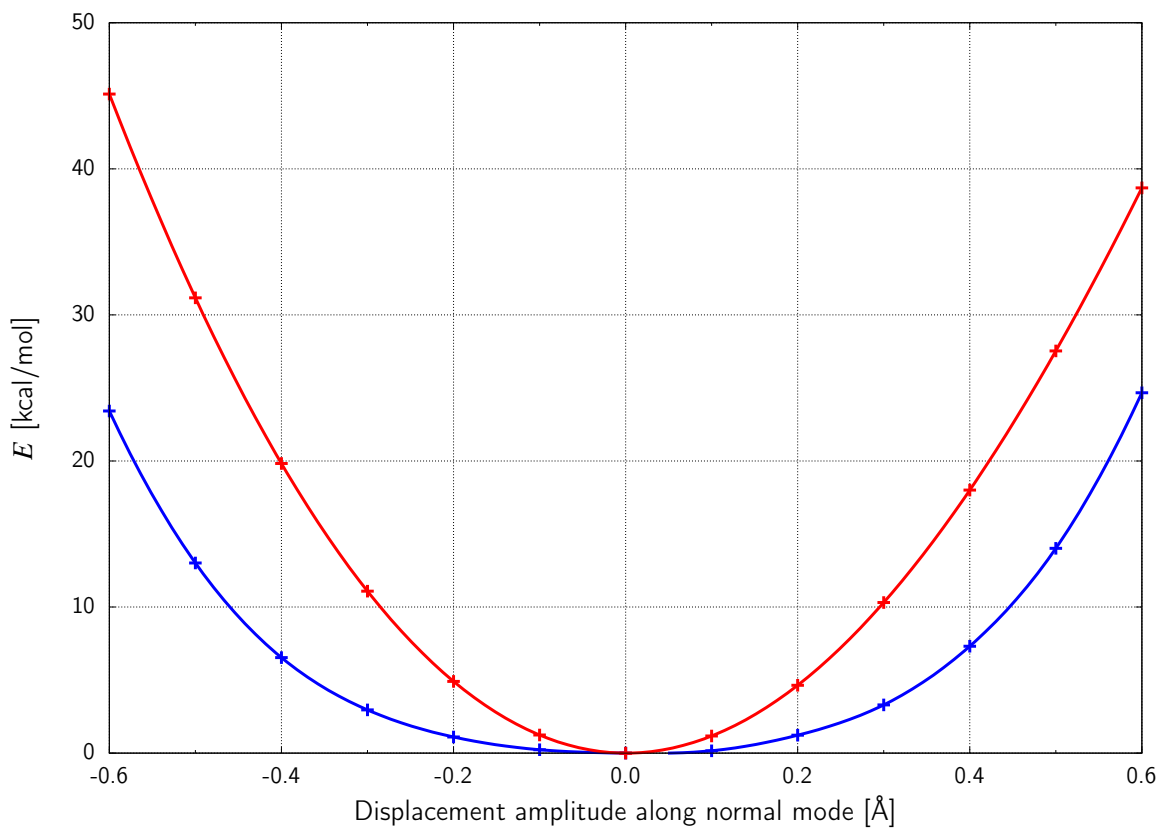


Figure 6: Variation of B3LYP/6-31+G(d) energy for Ti@C₂₈ as a function of the displacement of atoms from the equilibrium geometry along the selected low-frequency normal modes characterized by large amplitudes of Ti atom motions along principal symmetry axis ($v_3(a_1)$, red) and in the perpendicular xy plane (doubly degenerate $v_1(e)$, blue).

Graphical TOC Entry

